Published in final edited form as:

Nature. 2009 December 24; 462(7276): 1065–1069. doi:10.1038/nature08628.

Secreted Semaphorins Control Spine Distribution and Morphogenesis in the Postnatal CNS

Tracy S. Tran[1,2], **Maria E. Rubio**[3], **Roger L. Clem**[1,2], **Dontais Johnson**[1,2], **Lauren Case**[4], **Marc Tessier-Lavigne**[4,5], **Richard L. Huganir**[1,2], **David D. Ginty**[1,2,6], and **Alex L. Kolodkin**[1,2,6]

[1]Solomon H. Snyder Department of Neuroscience, The Johns Hopkins University School of Medicine, Baltimore, MD, 21205

[2]Howard Hughes Medical Institute, The Johns Hopkins University School of Medicine, Baltimore, MD, 21205

[3]Departments of Physiology and Neurobiology, University of Connecticut, Storrs, CT 06269

[4]Graduate Program in Neurosciences, Stanford University, Stanford, CA 94305

[5]Division of Research, Genentech, South San Francisco, CA 94080 USA

Abstract

The majority of excitatory synapses in the mammalian CNS are formed on dendritic spines1, and spine morphology and distribution are critical for synaptic transmission2–6, synaptic integration and plasticity7. Here, we show that a secreted semaphorin, Sema3F, is a negative regulator of spine development and synaptic structure. Mice with null mutations in genes encoding Sema3F, and its holoreceptor components neuropilin-2 (Npn-2) and plexinA3 (PlexA3), exhibit increased dentate gyrus (DG) granule cell (GC) and cortical layer V pyramidal neuron spine number and size, and also aberrant spine distribution. Moreover, Sema3F promotes loss of spines and excitatory synapses in dissociated neurons *in vitro*, and in *Npn-2*$^{-/-}$ brain slices cortical layer V and DG GCs exhibit increased mEPSC frequency. In contrast, a distinct Sema3A–Npn-1/PlexA4 signaling cascade controls basal dendritic arborization in layer V cortical neurons but does not influence spine morphogenesis or distribution. These disparate effects of secreted semaphorins are reflected in the restricted dendritic localization of Npn-2 to apical dendrites and of Npn-1 to all dendrites of cortical pyramidal neurons. Therefore, Sema3F signaling controls spine distribution along select dendritic processes, and distinct secreted semaphorin signaling events orchestrate CNS connectivity through the differential control of spine morphogenesis, synapse formation, and the elaboration of dendritic morphology.

[6]To whom correspondence should be sent: dginty@jhmi.edu and kolodkin@jhmi.edu.

Author Contributions

T.S.T. performed most of the experiments and data analysis, and M.E.R. performed most of the non-serial TEM analysis. R.L.C. and R.L.H. performed and analyzed whole cell patch recordings. L.C and M.T-L. participated in the analysis of *Plexin* mutant mice. D.J. provided technical support. T.S.T., D.D.G. and A.L.K. designed the experiments and wrote the manuscript.

Several axon guidance cues, including class 3 semaphorins (Sema3s), play key roles in synapse formation and function8–11. For example, Sema3A promotes the elaboration of dendrite complexity *in vitro*12, 13, may similarly affect dendritic spines14, and both Sema3A and Sema3F can regulate synaptic transmission in acute brain slices15, 16. Moreover, *Sema3F*$^{-/-}$ mutant mice exhibit seizures, and the Sema3F receptor Npn-2 is enriched in the postsynaptic density (PSD)15. We address here the *in vivo* roles for these guidance cues and their receptors in synaptogenesis.

Sema3F and its receptor Npn-2 are expressed during synaptogenesis in the hippocampus at postnatal day (P)21 (Supplementary Fig. 1). Npn-2 is enriched in the DG molecular layer, where dendrites of granule cells reside (Supplementary Fig. 1a). Sema3F is strongly expressed in the hilus, along the projection pathways of both supra- and infrapyramidal axons, and also along entorhinal cortex axons that innervate the DG molecular layers (Supplementary Fig. 1d). Therefore, Sema3F and Npn-2 are expressed in patterns consistent with these proteins directing postnatal hippocampal neural circuit formation.

To assess the involvement of Sema3A and Sema3F in the regulation of dendritic morphology and synaptogenesis we performed Golgi analysis on P14, P21 and adult brains of wild-type (WT) mice and mice harboring targeted mutations in genes encoding class 3 semaphorins and their receptors. We observed abnormal spine morphology and increased spine number in P21 and adult DG GCs in both *Sema3F*$^{-/-}$ and *Npn-2*$^{-/-}$ mutants (Fig. 1a–c, k; Supplementary Fig. 2h–j, n). Similar fully penetrant and expressive spine morphology defects were observed on apical dendrites of P21 (Supplementary Fig. 2k–m, n) and adult (Fig. 1d–f, j) cortical layer V pyramidal neurons in both *Sema3F*$^{-/-}$ and *Npn-2*$^{-/-}$ mutants. No abnormalities in spine density were observed in *Npn-2*$^{-/-}$ mutants at P14 in either DG GCs or layer V neurons (Supplementary Fig. 2d–g, n). Consistent with cortical neuron dendritic spine abnormalities in *Sema3F*$^{-/-}$ and *Npn-2*$^{-/-}$ mutants, we detected endogenous Npn-2 receptors in deep cortical layers and endogenous Sema3F ligand in both the P21 and adult neocortex (Supplementary Fig. 1g, h, j, k), suggesting Sema3F signals through its Npn-2 receptor to regulate spine morphogenesis.

We also observed aberrant spine distribution along apical dendrites of cortical layer V pyramidal neurons in adult *Sema3F*$^{-/-}$ and *Npn-2*$^{-/}$ mutant mice; 3.5-fold more spines were present on primary apical dendrites immediately proximal (0–50μm) to the cell soma, a location where few to no spines were found in WT animals (Fig. 1g–j). Analogous spine distribution abnormalities were observed in hippocampal DG GC primary dendrites (Fig. 1k; Supplementary Fig. 2 a–c). Spine number normally increases with distance from the soma in WT animals3. Spine distribution along the middle segments of primary dendrites of both layer V neurons and DG GCs was significantly altered in both *Sema3F*$^{-/-}$ and *Npn-2*$^{-/-}$ mutants (Fig. 1 a–f, j, k), however spine density and morphology along oblique (secondary) branches from primary apical dendrites, and along basal dendrites of layer V cortical neurons, were normal in *Sema3F*$^{-/-}$ and *Npn-2*$^{-/-}$ mutants (Supplementary Fig. 3). Spine number and morphology on both apical and basal dendrites of hippocampal CA1 and cortical layer II/III pyramidal neurons were normal in *Sema3F*$^{-/-}$ and *Npn-2*$^{-/-}$ mutants (Supplementary Fig. 4). Therefore, Sema3F–Npn-2 signaling restricts dendritic spine

number, distribution, and regulates spine morphology in select neuronal populations and within distinct dendritic compartments.

We next used a rescue paradigm employing *in utero* electroporation to deliver a *Npn-2-IRES-mGFP* expression construct to a small number of cortical layer V pyramidal neurons in the *Npn-2*$^{-/-}$ mutant cortex at embryonic day 13.5 (E13.5), when deep layer cortical neurons are born. Spine density along apical dendrites was assessed in GFP^{+} neurons between P35–45. *Npn-2*$^{-/-}$ layer V pyramidal neurons expressing mGFP alone exhibited numerous, aberrant spines along their apical dendrites (Fig. 2a, b, d). In contrast, *Npn-2*$^{-/-}$ cortical neurons harboring the *Npn-2-IRES-mGFP* construct had 39% fewer spines than *Npn-2*$^{-/-}$ cortical neurons expressing mGFP alone (Fig. 2c, d). Thus, Npn-2 controls spine number and morphology in a cell-autonomous manner.

To assess the influence of Sema3F on excitatory synapses we treated dissociated cultured WT P5 DG neurons with recombinant Sema3F, followed by immunolabeling for the pre- and postsynaptic markers vGlut1 and PSD-95, respectively (Supplementary Fig. 5a–c). Sema3F decreased the average number of puncta exhibiting co-localization of vGlut-1 and PSD-95 by ~50%, however Sema3A treatment had no effect (Supplementary Fig. 5d). No significant effect on the number of vGlut1 puncta was observed following Sema3F treatment, however the number of PSD-95–positive puncta decreased by ~40% following Sema3F treatment compared to untreated, or Sema3A-treated, neurons (Supplementary Fig. 5e). The majority of PSD-95-positive puncta in untreated cultured neurons were colocalized with presynaptic vGlut1, and the decrease in the number of excitatory synapses (colocalized vGlut1/PSD-95) was reflected in the decrease in total PSD-95-positive puncta. Sema3F treatment did not affect DG inhibitory synapses (Supplementary Fig. 5f–i). Therefore, Sema3F negatively and selectively influences excitatory synapses. We performed whole cell voltage clamp recordings to assess mEPSCs in layer V pyramidal neurons and DG GCs in acute brain slices derived from 3–4 week-old *Npn-2*$^{-/-}$ and WT mice (Fig. 2e and Supplementary Fig. 6). We observed a 2.4 and 1.5 fold increase in mEPSC frequency in *Npn-2*$^{-/-}$ layer V neurons and DG GCs, respectively, as compared to WT littermates. Although we observed a slight decrease in the rise time and tau decay for layer V neurons, no significant change in amplitude was observed compared to WT littermates (Fig. 2e and Supplementary Fig. 6a). No significant difference in the paired pulse amplitude ratio was observed between *Npn-2*$^{-/-}$ and WT neurons from layer V or DG (Supplementary Fig. 6), suggesting that the increase in mEPSC frequency found in *Npn-2*$^{-/-}$ mutant mice is due to an increase in the number of synapses rather than an increase in the probability of presynaptic release. These results show that Sema3F–Npn-2 signaling negatively regulates both excitatory synapse number and synaptic transmission in layer V and DG neurons.

To determine how loss of *Sema3F* and *Npn-2* influences synapse formation *in vivo*, we used transmission electron microscopy (TEM) to visualize dendritic spine ultrastructure and excitatory synapse morphology. Spines protruding from the dendritic shafts of WT adult DG GCs are small (<0.1 μm^2), and of the >270 spines scored (per genotype) we observed that most have round, uniformly shaped, spine heads (Fig. 3a). In contrast, spines in *Sema3F*$^{-/-}$ and *Npn-2*$^{-/-}$ mutants are enlarged, vary greatly in shape, and exhibit a >1.7-fold increase in area as compared to WT spines (Fig. 3a, b; Supplementary Fig. 7a, c, d, f). In spines of

mutant mice we observed pre- and postsynaptic components normally associated with WT synapses, including electron dense membranous folds in the postsynaptic density (PSD), vesicle pools near active zones, and docked vesicles associated with presynaptic termini (Fig. 3a, b; Supplementary Fig. 7c, d). However, in adult *Sema3F*$^{-/-}$ and *Npn-2*$^{-/-}$ mice we observed a ~5-fold increase in the fraction of DG GC spines harboring multiple PSDs (Fig. 3b; Supplementary Fig. 7c, g). Serial section EM reconstructions of several mutant DG GC spines showed that these are perforated PSDs contacted by the same presynaptic terminal (Fig. 3c, d). We found similarly pronounced cortical layer V neuron spine and synaptic morphology defects at the ultrastructural level in both *Sema3F*$^{-/-}$ and *Npn-2*$^{-/-}$ mutants (Supplementary Fig. 8). Since spine stability, maturation and number increase with age17, 18, we asked whether these abnormalities observed in adult *Sema3F*$^{-/-}$ and *Npn-2*$^{-/-}$ mice result from altered spine morphogenesis. Indeed, spines along P21 DG GC dendrites in *Npn-2*$^{-/-}$ animals already exhibit aberrant morphology similar to that seen in adult *Npn-2*$^{-/-}$ mutants (Supplementary Fig. 9). These TEM analyses demonstrate that Sema3F and Npn-2 regulate spine morphogenesis and postsynaptic specializations, serving to constrain overall spine number, size, and PSD number.

Npns in combination with a class A plexin signaling receptor constitute most secreted semaphorin holoreceptors, and Sema3A preferentially signals through a Npn-1/PlexA4 holoreceptor while Sema3F signals through a Npn-2/PlexA3 holoreceptor19–21. Analysis of Golgi-labeled adult *PlexA3*$^{-/-}$ and *PlexA4*$^{-/-}$ mutant brains revealed that apical dendrite spine morphology is dramatically altered in *PlexA3*$^{-/-}$, but not *PlexA4*$^{-/-}$, layer V cortical pyramidal neurons (Fig. 4a, a', b–d'; Supplementary Fig. 10a), similar to what we observed in *Sema3F*$^{-/-}$ and *Npn-2*$^{-/-}$ mutants (Fig. 1d–f). DG GC dendritic spines in both *PlexA3*$^{-/-}$ and *PlexA4*$^{-/-}$ mutants are larger, more numerous, and extend much further from the GC dendrite shaft than WT spines (Supplementary Fig. 11a–d). TEM ultrastructural analysis of *PlexA3*$^{-/-}$ and *PlexA4*$^{-/-}$ mice also revealed enlarged and irregularly shaped DG GC spines (Supplementary Fig. 7a, b, e–g). The requirement for PlexA3 and PlexA4 for normal DG GC spine morphology is reminiscent of the requirement for both plexins *in vivo* for correct guidance and extension of embryonic trigeminal neurons, and *in vitro* for repulsive responses to high levels of Sema3A21.

Mice homozygous for a knock-in mutation that expresses a Npn-1 protein incapable of binding to Sema3A (*Npn-1*$^{Sema-}$) phenocopy embryonic neuronal defects observed in *Npn-1* null mice and exhibit dramatically reduced growth and branching of layer V cortical neuron basal dendritic arbors12. Moreover, acute application of Sema3A to WT brain slices promotes an increase in growth and branching of basal dendritic arbors13. However, *Npn-1*$^{Sema-}$ (Fig. 4a, a', c, c'; Supplementary Fig. 10a) and *Sema3A*$^{-/-}$ (not shown) mice do not exhibit spine density defects along apical dendrites of cortical layer V neurons. These results show that Sema3A–Npn-1 signaling positively regulates dendrite growth and branching, but they do not address whether plexin signaling underlies these functions or whether defects in spine morphology in *Sema3F*, *Npn-2*, and *PlexA3* mutants are correlated with other dendrite morphogenesis defects. Therefore, we performed Golgi staining on adult brains from WT, *Sema3A*$^{-/-}$, *Sema3F*$^{-/-}$, *Npn-1*$^{Sema-}$, *Npn-2*$^{-/-}$, *PlexA3*$^{-/-}$ and *PlexA4*$^{-/-}$ mice. Dendrite orientation and branching in DG GCs in all mutants analyzed was identical

to WT (Supplementary Fig. 11e–k). Layer V cortical neuron basal dendrites were also similar to WT in *Sema3F*$^{-/-}$, *Npn-2*$^{-/-}$ and *PlexA3*$^{-/-}$ mutants (Fig. 4a, b; *Sema3F*$^{-/-}$ and *Npn-2*$^{-/-}$ not shown). However, *Npn-1*$^{Sema-}$, *PlexA4*$^{-/-}$, and *Sema3A*$^{-/-}$ mice exhibited severe reductions (~3.8-fold at 63 μm from the cell soma) in the elaboration of basal dendrites of these cortical pyramidal neurons as compared to WT (Fig. 4a, c, d; Supplementary 10b; *Sema3A*$^{-/-}$ not shown). Therefore, spine defects observed along layer V cortical apical dendrite processes in *Sema3F*, *Npn-2*, and *PlexA3* mutant mice are not correlated with the basal dendritic arbor phenotypes observed in the *PlexA4*$^{-/-}$, *Npn-1*$^{Sema-}$, and *Sema3A*$^{-/-}$ mutants12, 13, thus revealing distinct functions of Sema3A–Npn-1/PlexA4 signaling in the promotion of basal dendrite complexity, and of Sema3F–Npn-2/PlexA3 in constraining spine number, distribution and synaptic transmission.

To ask how distinct Sema3 signaling pathways independently regulate cortical neuron basal dendrite morphology and apical dendrite spine morphogenesis, we examined subcellular Npn receptor distribution on dissociated E14.5 cortical neurons grown for 18 DIV using AP-Sema3F (to reveal cell surface Npn-2) and AP-Sema3A (to reveal Npn-1). We observed that cell surface Npn-2 receptors were predominantly localized to the primary apical dendrite in cortical neurons with pyramidal morphology (Fig. 5a–f, j); Npn-2 was absent from both basal dendrites and oblique, or secondary, branches off of primary apical dendrites in these neurons (Fig. 5a, d, k and Supplementary Fig. 12b). This observation was confirmed using Npn-2 antibodies (Supplementary Fig. 11a–a’’’). Npn-1 receptors, in contrast, were more uniformly distributed on all dendritic processes (Fig. 5g–i, j). This exquisite pattern of Npn-2 distribution likely explains the restricted effects of Sema3F on spines associated with primary apical dendrites (Fig. 1j and Supplementary Fig. 3h).

To ask whether Sema3F–Npn-2 signaling can directly regulate cortical neuron spine density and morphology, we next employed an assay in which dendritic spines are visualized following transfection of primary neuronal cultures derived from mouse E14.5 neocortex with an IRES-myristoylated GFP (mGFP) construct (Supplementary Fig. 13a). Sema3F-treated WT cortical neurons with pyramidal morphology have along their apical, but not basal, dendrites 33% fewer spines than do untreated (control) or Sema3A-treated neurons (Supplementary Fig. 13b–c, j). In contrast, *Npn-2*$^{-/-}$ cortical neurons transfected with *IRES-mGFP* displayed a similar number of spines along their apical dendritic process in both untreated and Sema3F-treated cultures (Supplementary Fig. 13d, e, j). However, *Npn-2*$^{-/-}$ cortical neurons transfected with a *Npn-2–IRES-mGFP* construct and subsequently treated with Sema3F have 24% fewer spines along their apical dendrites as compared to untreated *Npn-2*$^{-/-}$ neurons (Supplementary Fig. 13f, g, j). Overexpression of Npn-2 using *Npn-2-IRES-mGFP* in WT dissociated cortical neurons produced no difference in apical or basal dendritic spine number, as compared to WT neurons transfected with *IRES-mGFP* (Supplementary Fig. 14a, c, e). However, Sema3F treatment of WT neurons over-expressing Npn-2 led to a 30% and 23% reduction in apical and basal dendritic spines, respectively, as compared to untreated neurons (Supplementary Fig. 13b, d, e).

The Npn-2 intracellular domain contains a C-terminal PDZ ligand motif (SEA) that may be critical for Npn-2/PlexA3 localization and Sema3F/Npn-2–mediated regulation of spine morphology and synapse structure. We transfected dissociated *Npn-2*$^{-/-}$ cortical neurons

with a Npn-2 SEA-deletion expression construct (*Npn-2-ΔSEA-IRES-mGFP*) and assessed Sema3F effects on spine morphology. *Npn-2-IRES-mGFP* and *Npn-2-ΔSEA-IRES-mGFP* constructs both promote expression of Npn-2 protein on the cell surface of *Npn-2*$^{-/-}$ cortical neurons (Supplementary Fig. 12d, e). However, *Npn-2*$^{-/-}$ neurons transfected with *Npn-2-ΔSEA-IRES-mGFP* do not exhibit a reduction in spine density following Sema3F treatment (Fig. 13h-j). Therefore, Sema3F-mediated reduction in spine number along cortical dendritic processes is dependent upon the Npn-2 cytoplasmic SEA PDZ domain-binding motif.

We demonstrate here that spatially segregated secreted semaphorin signaling orchestrates the elaboration of distinct morphological features in select hippocampal and cortical pyramidal neuron dendrites. The organization and distribution of excitatory synapses along primary, secondary and higher order dendritic branches defines how presynaptic inputs are integrated into neural networks. Thus, the precise control of both excitatory and inhibitory synapse distribution during neural development is essential for the formation of functional circuits. Our finding that Sema3F orchestrates the spatial distribution of spines along apical dendrites of cortical pyramidal and hippocampal granule neurons suggests that this secreted cue is essential for integration of excitatory inputs onto these neurons. Supporting this idea, both cortical and hippocampal neurons from *Npn-2*$^{-/-}$ mutant mice exhibit an increased mESPC frequency, and we observed previously that mice lacking components of the Sema3F–Npn-2/PlexA3 signaling module exhibit alterations in synaptic transmission and seizures15. These findings underscore the necessity of understanding the mechanisms underlying Sema3F–Npn-2/PlexA3 control of differential spine growth and distribution, and Sema3A–Npn-1/PlexA4 control of basal dendrite growth. Npn-2 is localized to the PSD15 and we show here that the Npn-2 PDZ domain-binding motif is essential for Sema3F responsiveness. The precise localization of Sema3 holoreceptor complexes via one or more PDZ scaffold proteins associated with postsynaptic components may serve to provide directed Sema3 signaling to subcellular dendritic compartments, regulating dendritic spine morphology and spatial distribution of synapses.

Methods Summary

The day when a vaginal plug was observed is designated as embryonic day (E) 0.5 and the day of birth as postnatal (P) day 0. Golgi labeling was performed as described (FD NeuroTechnologies). For *in utero* electroporation, E13.5 embryos from timed-pregnant WT and *Npn-2*$^{-/-}$ females from homozygous crosses were used. WT P5 dentate gyrus hippocampi, and WT or *Npn-2*$^{-/-}$ E14.5 cortices, were dissected and dissociated for primary culture experiments. See Supplemental Methods for additional experimental procedures, including: TEM, serial 3-D reconstruction, immunocytochemistry, physiological recordings, and quantification parameters for spine density, synaptic puncta, Sholl analysis, and AP-fluorescence.

Supplementary Material

Refer to Web version on PubMed Central for supplementary material.

Acknowledgements

We thank Michael Delannoy and the Johns Hopkins University School of Medicine Microscope Facility for assistance with EM analysis; Michele Pucak and the NINDS Multi-photon Core Facility at JHMI; Dwight Bergles and David Linden for comments on the manuscript; Rafael Yuste for helpful discussions; Kayam Chak and members of the Kolodkin and Ginty laboratories for assistance throughout the course of this project. This work was supported by R01 MH59199 to DDG and ALK; NRSA F32 NS051003 to TST; R01 DC-006881 and NSF DB1-0420580 to MER; and P50 MH06883 to RLH and DDG. DDG, RLH and ALK are investigators of the Howard Hughes Medical Institute.

References

1. Nimchinsky E, Sabatini B, Svoboda K. Structure and function of dendritic spines. Annu Rev Physiol. 2002; 64:313–353. [PubMed: 11826272]
2. Elston G, Defelipe J. Spine distribution in cortical pyramidal cells: a common organizational principle across species. Prog Brain Res. 2002; 136:109–133. [PubMed: 12143375]
3. Ballesteros-Yáñez I, Benavides-Piccione R, Elston G, Yuste R, Defelipe J. Density and morphology of dendritic spines in mouse neocortex. Neuroscience. 2006; 138:403–409. [PubMed: 16457955]
4. Hayashi Y, Majewska A. Dendritic spine geometry: functional implication and regulation. Neuron. 2005; 46:529–532. [PubMed: 15944122]
5. Alvarez V, Sabatini B. Anatomical and physiological plasticity of dendritic spines. Annu Rev Neurosci. 2007; 30:79–97. [PubMed: 17280523]
6. Gao W-J, Zheng Z-H. Target-specific differences in somatodendritic morphology of layer V pyramidal neurons in rat motor cortex. J Comp Neurol. 2004; 476:174–185. [PubMed: 15248197]
7. Spruston N. Pyramidal neurons: dendritic structure and synaptic integration. Nat Rev Neurosci. 2008; 9:206–221. [PubMed: 18270515]
8. McAllister A. Dynamic Aspects of CNS Synapse Formation. Annu Rev Neurosci. 2007; 30:425–450. [PubMed: 17417940]
9. Packard M, et al. The Drosophila Wnt, wingless, provides an essential signal for pre- and postsynaptic differentiation. Cell. 2002; 111:319–330. [PubMed: 12419243]
10. Poon V, Klassen M, Shen K. UNC-6/netrin and its receptor UNC-5 locally exclude presynaptic components from dendrites. Nature. 2008; 455:669–673. [PubMed: 18776887]
11. Pasterkamp R, Giger R. Semaphorin function in neural plasticity and disease. Curr Opin Neruobiol. 2009; 19:263–274.
12. Gu C, et al. Neuropilin-1 conveys semaphorin and VEGF signaling during neural and cardiovascular development. Dev. Cell. 2003; 5:45–57. [PubMed: 12852851]
13. Fenstermaker V, Chen Y, Ghosh A, Yuste R. Regulation of dendritic length and branching by semaphorin 3A. J Neurobiol. 2004; 58:403–412. [PubMed: 14750152]
14. Yamashita N, et al. Regulation of spine development by Semaphorin3A through Cyclin-Dependent Kinase 5 phosphorylation of Collapsin Response Mediator Protein 1. J Neurosci. 2007; 27:12546–12554. [PubMed: 18003833]
15. Sahay A, et al. Secreted semaphorins modulate synaptic transmission in the adult hippocampus. J Neurosci. 2005; 25:3613–3620. [PubMed: 15814792]
16. Bouzioukh F, et al. Semaphorin3A regulates synaptic function of differentiated hippocampal neurons. Euro. J. Neurosci. 2006; 23:2247–2254.
17. Yuste R, Bonhoeffer T. Genesis of dendritic spines: insights from ultrastructural and imaging studies. Nat Rev Neurosci. 2004; 5:24–34. [PubMed: 14708001]
18. Zuo Y, Lin A, Chang P, Gan W. Development of long-term dendritic spine stability in diverse regions of cerebral cortex. Neuron. 2005; 46:181–189. [PubMed: 15848798]
19. Cheng H, et al. Plexin-A3 mediates semaphorin signaling and regulates the development of hippocampal axonal projections. Neuron. 2001; 32:249–263. [PubMed: 11683995]
20. Suto F, et al. Plexin-a4 mediates axon-repulsive activities of both secreted and transmembrane semaphorins and plays roles in nerve fiber guidance. J Neurosci. 2005; 25:3628–3637. [PubMed: 15814794]

21. Yaron A, Huang PH, Cheng HJ, Tessier-Lavigne M. Differential requirement for Plexin-A3 and -A4 in mediating responses of sensory and sympathetic neurons to distinct class 3 Semaphorins. Neuron. 2005; 45:513–523. [PubMed: 15721238]

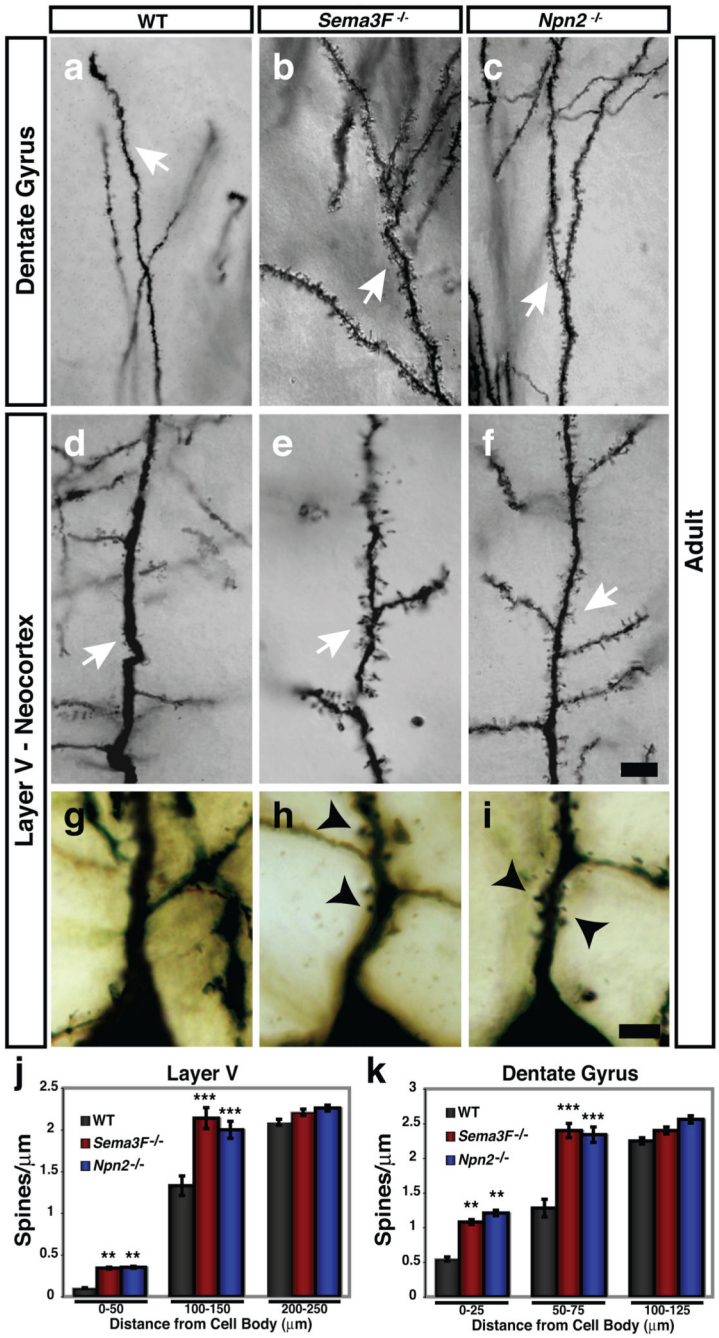

Figure 1. Sema3F and Npn-2 regulate dendritic spine number, distribution and morphology in adult layer V pyramidal neurons and dentate gyrus granule cells *in vivo*

a–f, Golgi stained *Sema3F*$^{-/-}$ (**b, e**) and *Npn-2*$^{-/-}$ (**c, f**) brains show that DG GC and layer V pyramidal apical dendritic spines (white arrows) are more numerous as compared to WT (**a, d**). **g–i**, Layer V pyramidal neurons have more spines on primary apical dendrites 0–25 μm from the soma in *Sema3F*$^{-/-}$ (**h**) and *Npn-2*$^{-/-}$ (**i**) mutants as compared to WT mice (**g**). **j, k**, Quantification of spine density 0–50μm from the cell body on layer V pyramidal primary apical dendrites (WT, 0.10 ±0.01; *Sema3F*$^{-/-}$, 0.34 ±0.01; *Npn-2*$^{-/-}$, 0.35 ±0.01 spines/μm)

and 0–25μm from the cell body on DG GC primary dendrites (WT, 0.55 ±0.03; *Sema3F*$^{-/-}$, 1.08 ±0.04 and *Npn-2*$^{-/-}$, 1.21 ±0.04 spines/μm). There is a significant increase in spine number on dendritic segments located 100–150μm from the cell body in layer V (WT, 1.33 ±0.14; *Sema3F*$^{-/-}$, 2.14 ±0.13; *Npn-2*$^{-/-}$, 2.00 ±0.11 spines/μm) and 50–75μm from the DG neuron cell body (WT, 1.28 ±0.13; *Sema3F*$^{-/-}$, 2.40 ±0.11; *Npn-2*$^{-/-}$, 2.34 ±0.12 spines/μm) in these mutants. There is no significant difference in spine density at 200–250μm or 100–125μm from the cell body in layer V and DG neurons, respectively. Error bars, ±SEM, ANOVA, post-hoc Tukey in **j** and **k**; **, p=0.01; ***, p=0.001 compared to WT. Scale bars: 10 μm in **f** for **a–f** and 2.5 μm in **i** for **g–i**.

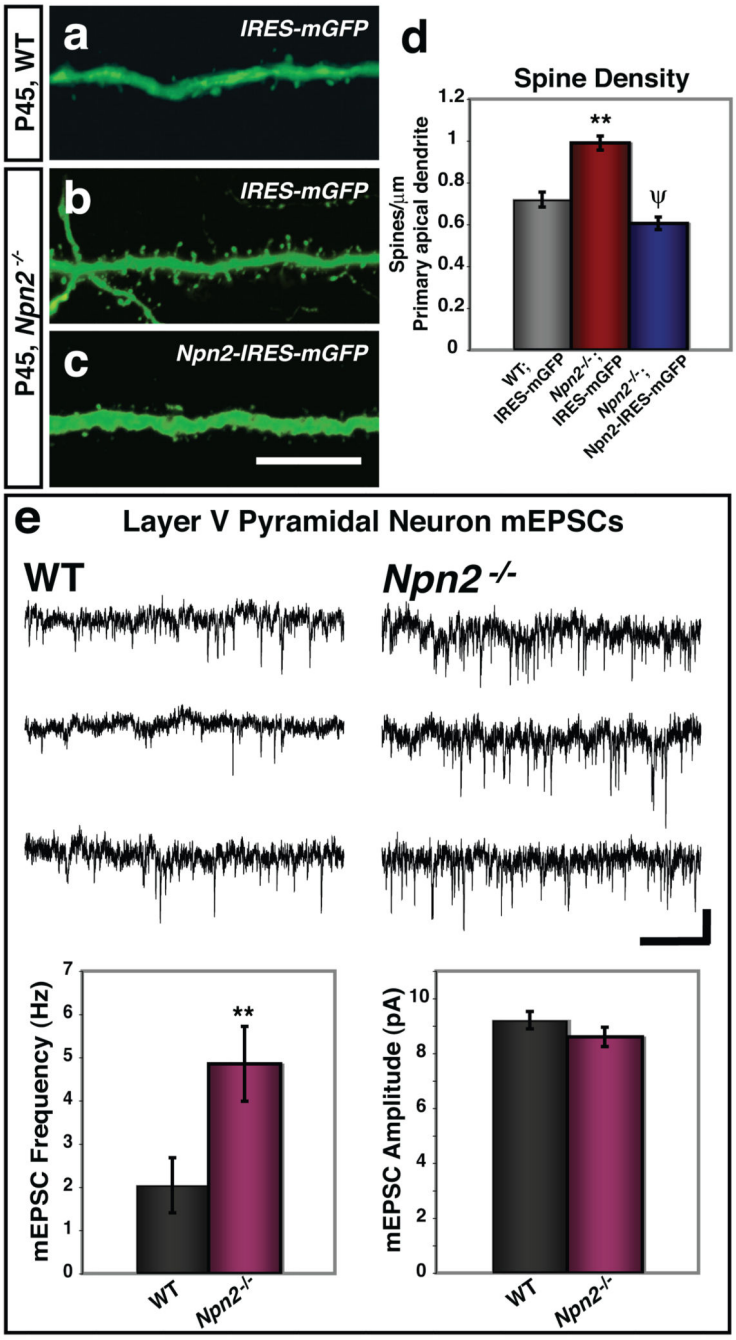

Figure 2. Sema3F–Npn-2 control of spine number is Npn-2 cell-autonomous, and *Npn-2* loss-of-function results in increased frequency of mEPSCs

a–c, Layer V neurons from P45 WT and *Npn-2*$^{-/-}$ animals from E13.5 embryos *in utero* electroporated with *IRES-mGFP* (**a, b**), and a *Npn-2*$^{-/-}$ embryo electroporated with *Npn-2-IRES-mGFP* (**c**). **d**, Quantification of spine density (50–100µm from soma) in *Npn-2*$^{-/-}$ neurons transfected with *Npn-2-IRES-mGFP* (0.61 ±0.03 spines/µm) as compared to *IRES-mGFP* (0.99 ±0.03 spines/µm), and to WT neurons transfected with *IRES-mGFP* (0.72 ±0.04 spines/µm). **e**, Recordings of mEPSCs from cortical slices show a significant increase

in mEPSC frequency in *Npn-2*$^{-/-}$ layer V pyramidal neurons (4.85 ±0.87 Hz) as compared to WT littermates (2.04 ±0.64 Hz). There is no significant difference in mEPSC amplitude between WT (9.21 ±0.32 pA) and *Npn-2*$^{-/-}$ (8.60 ±0.35 pA) neurons. Representative mEPSC traces (top, WT; bottom, *Npn-2*$^{-/-}$) are shown. Error bars in **d** and **e**, ±SEM; ANOVA, post-hoc Tukey for **d**; p=0.001 for **, WT:*IRES-mGFP* vs. *Npn-2*$^{-/-}$:*IRES-mGFP* and ψ, *Npn-2*$^{-/-}$:*IRES-mGFP* vs. *Npn-2*$^{-/-}$:*Npn-2-IRES-mGFP*; p=0.071 for WT vs. *Npn-2*$^{-/-}$:*Npn-2-IRES-mGFP*. T-test for **e**, **, p=0.024 for frequency and p=0.231 for amplitude. Scale bars: 10 μm in **c** for **a**–**c**, and 5 pA × 1s in **e**.

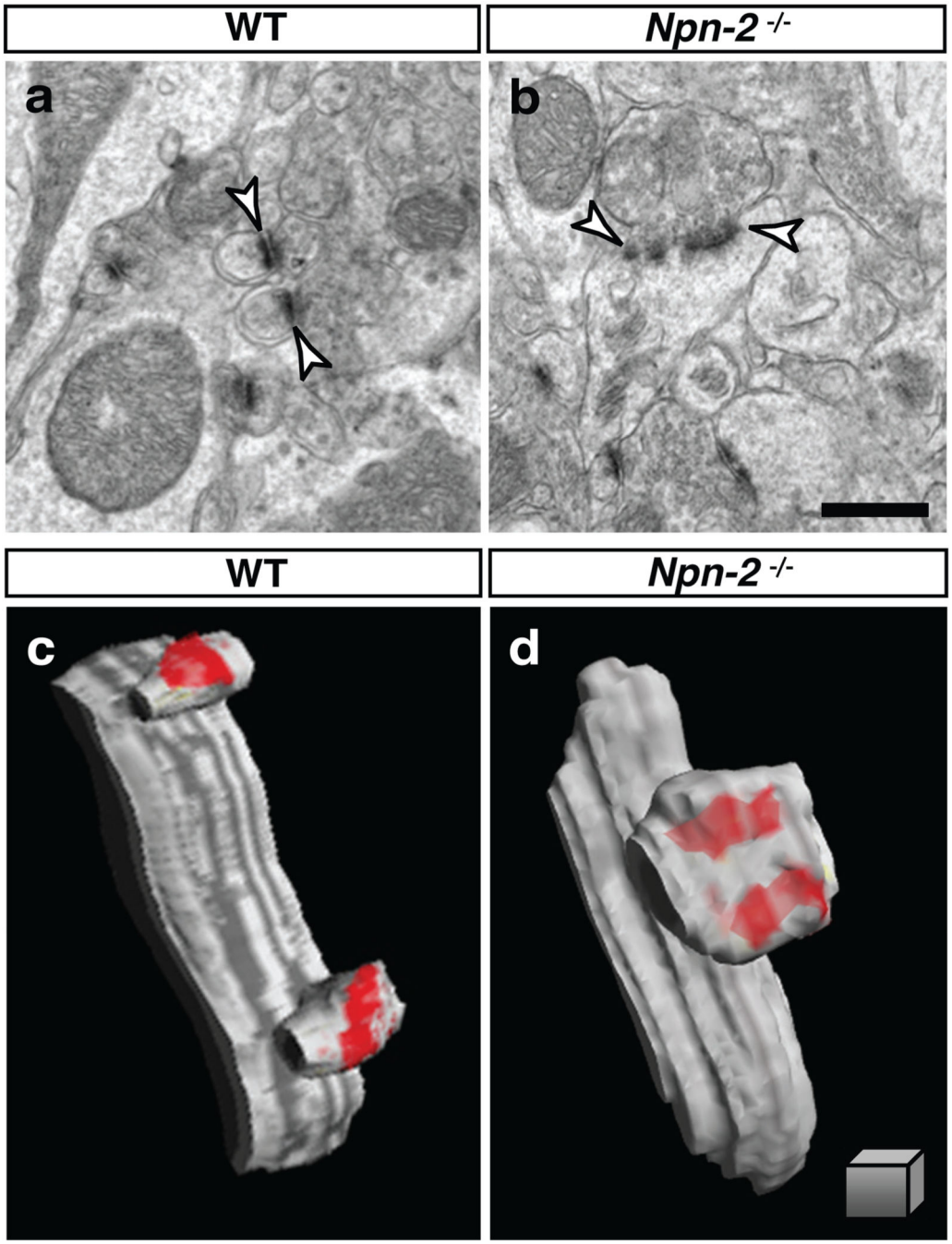

Figure 3. Sema3F-Npn2 signaling regulates spine morphology and synaptic ultrastructure *in vivo*

a, b, DG GC dendritic spine TEM ultrastructural analysis reveals enlarged and misshapen spines (arrowheads) in *Npn2*$^{-/-}$ (**b**) as compared to WT mice (**a**). **c, d**, 3-D reconstructions of serial TEM illustrates two completely separate PSDs within a single spine from a *Npn-2*$^{-/-}$ mutant mouse (**d**), in contrast to a WT spine (**c**) with one PSD per spine head. Scale bars: 500 nm in **b** for **a, b**, and 250 nm^3 in **d** for **c, d**

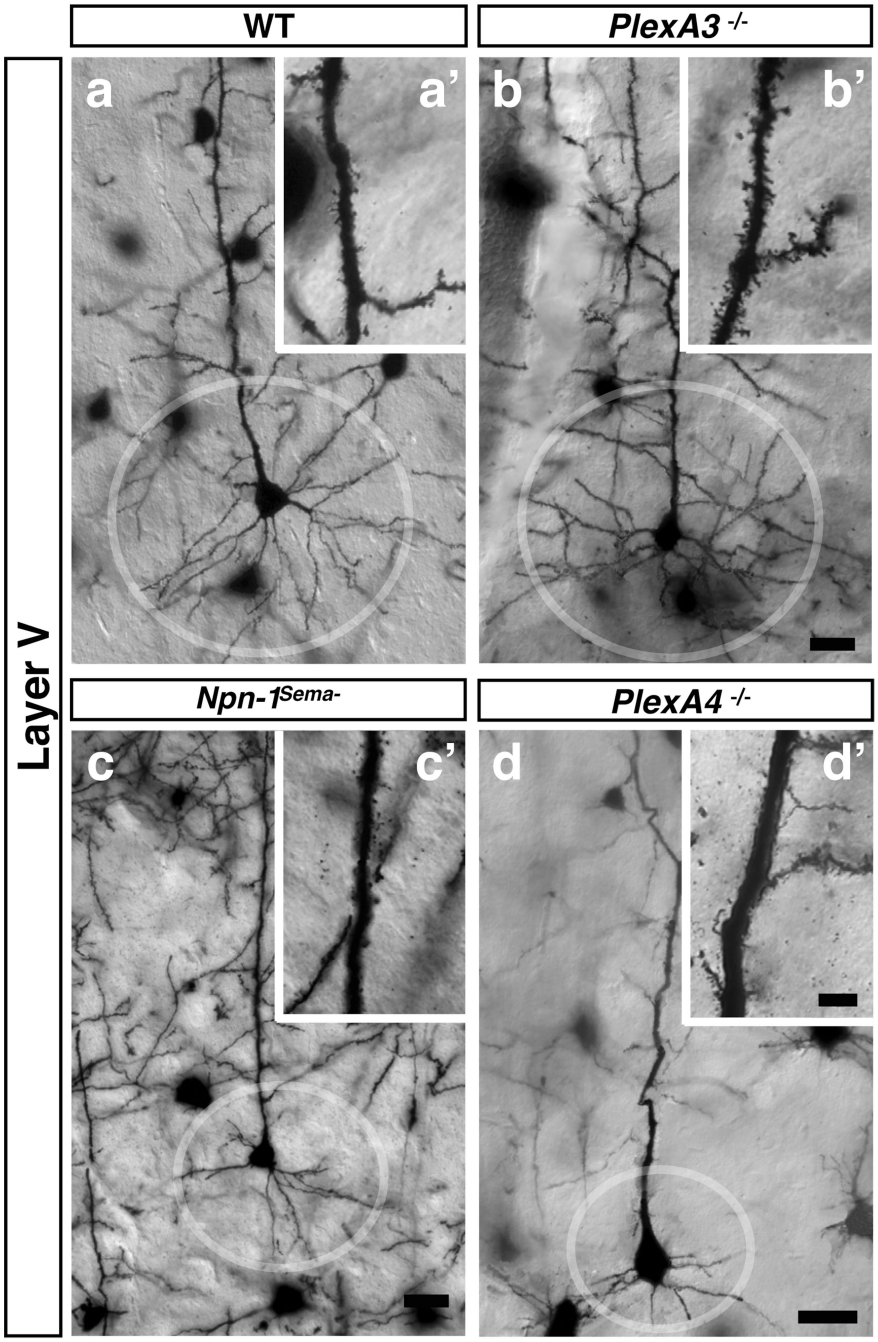

Figure 4. Distinct Sema3–Npn/PlexA signaling modules regulate apical dendrite spine morphology and basal dendrite process complexity

a–d, Golgi-labeled adult brains illuminate basal dendritic morphologies in cortical layer V pyramidal neurons from WT (**a**, circle), *PlexA3*$^{-/-}$ (**b**), *Npn-1*$^{Sema-}$ (**c**), and *PlexA4*$^{-/-}$ (**d**) mice. **a'–d'**, show spine morphologies from neurons in **a–d**. Scale bars: 10 μm in **d** for **a–d** and 4 μm in **d'** for **a'–d'**.

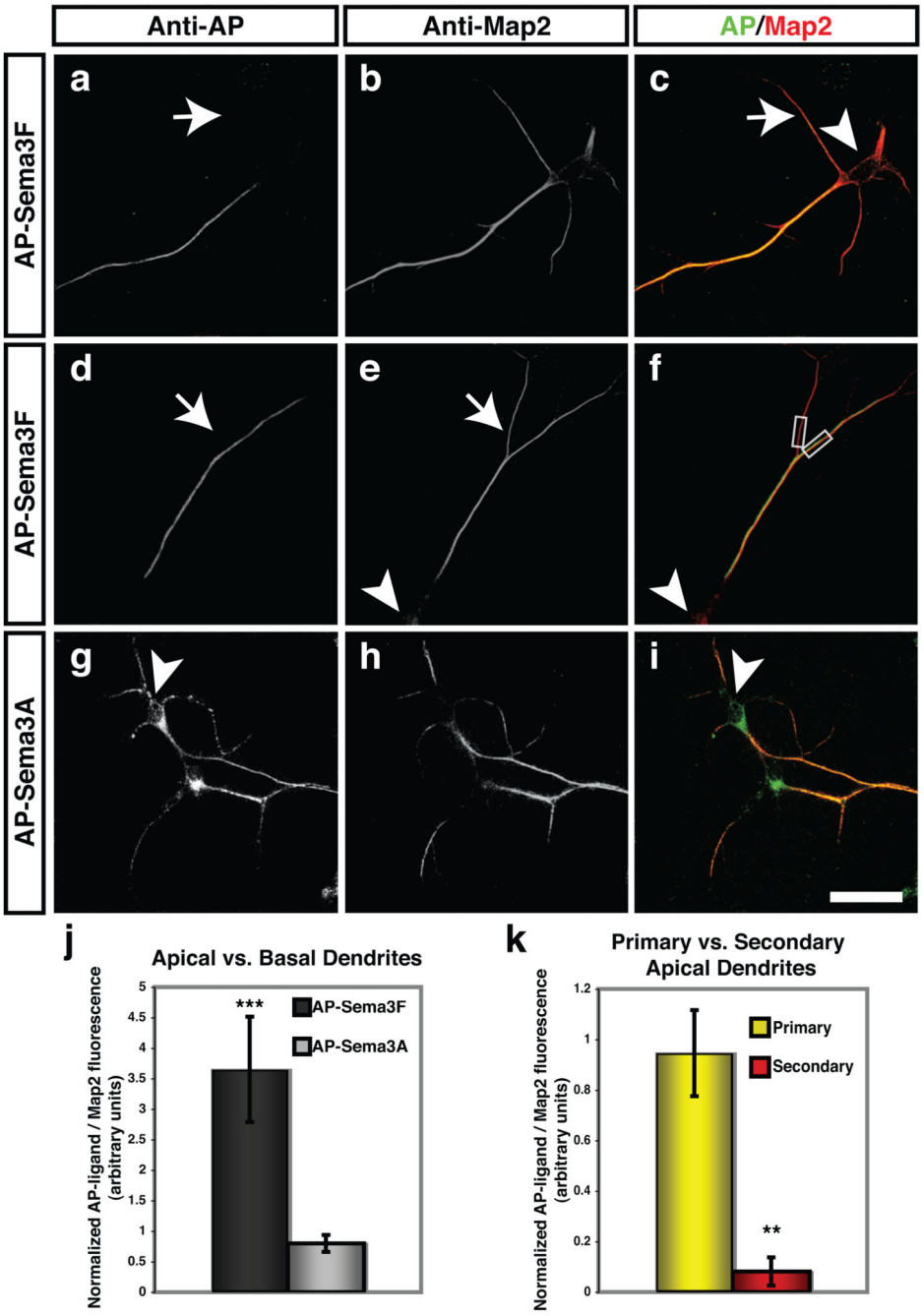

Figure 5. Npn-1 and Npn-2 are localized to distinct cortical pyramidal neuron dendritic domains

a–i, Alkaline phosphatase (AP)-Sema3F (**a–f**) or AP-Sema3A (**g–i**) fusion proteins were used to localize endogenous Npn-2 and Npn-1, respectively, on cortical pyramidal neurons in primary culture. Endogenous Npn-2 (**a, c, d, f**) is predominately restricted to the major apical dendrites of pyramidal neurons as shown by anti-AP labeling (**a–c**). Npn-2 is not observed on basal (white arrows in **a**, **c**) or secondary apical dendritic branches (white arrows in **d**, **e**) illuminated by anti-Map2 staining. Npn-1 (**g, i**) is observed on basal and apical dendritic processes (**h, i**). **j, k**, Fluorescence intensities were quantified by measuring

apical/basal fluorescence ratios and normalizing to apical/basal Map2 fluorescence ratios for AP-Sema3F–labeled neurons (**j**, 3.70 ±0.87), and for AP-Sema3A–labeled neurons (0.80 ±0.14). The Npn-2/Map2 fluorescence ratio in primary apical dendrites (yellow bar, **k**) is 0.95 (±0.17), and in secondary apical dendrites (red bar, **k**) is 0.08 (±0.06). Gray boxes, **f**, indicate area of measurement in **k**. Scale bars: 25 μm in **i** for **a–i**.